EUROPEAN ORGANIZATION FOR NUCLEAR RESEARCH

CERN/EP 81-68 Rev.
2 July 1981

STUDY OF HADRONIC EVENTS IN pp COLLISIONS AT $\sqrt{s}$ = 62 GeV AND COMPARISON WITH HADRONIC EVENTS IN e^+e^- COLLISIONS

A. Breakstone, H.B. Crawley, A. Firestone, M. Gorbics, J.W. Lamsa, W.T. Meyer, and D.L. Parker
Department of Physics and Ames Laboratory, Iowa State University, Ames, USA

D. Drijard, F. Fabbri(*), H.G. Fischer, H. Frehse, P. Hanke, P.G. Innocenti, and O. Ullaland
CERN, European Organization for Nuclear Research, Geneva, Switzerland

W. Hofmann, M. Panter, K. Rauschnabel, J. Spengler and D. Wegener
Institut für Physik der Universität Dortmund, Dortmund, Germany

W. Geist, M. Heiden, E.E. Kluge, T. Nakada and A. Putzer
Institut für Physik der Universität Heidelberg, Heidelberg, Germany

K. Doroba, R. Gokieli and R. Sosnowski
Institute for Nuclear Research, Warsaw, Poland

ABSTRACT

We present an analysis of minimum bias events from proton-proton collisions at $\sqrt{s}$ = 62 GeV in the CERN ISR. We remove the effects of both the leading protons and compare the B = 0 mesonic residue of the events to the hadronic events of similar energy produced in e^+e^- collisions. This comparison is presented in terms of the standard jet-type analyses involving quantities such as sphericity and aplanarity. We find significant differences between these data and the data from e^+e^- annihilations. The data of this experiment are consistent with the predictions of a longitudinal phase space model.

Submitted to Zeitschrift für Physik C

(*) Visitor from INFN, Bologna, Italy.

0416P/AF/ed

Since the discovery of jets in e^+e^- annihilation into hadrons [1], compelling evidence has been presented for the two-jet structure of e^+e^- annihilation into hadrons [2]. More recently, evidence has been presented for the presence of a three-jet signal in such events, [3] which has been interpreted as evidence for the presence of gluons. By contrast there is very little evidence for the presence of jets from parton scattering in purely hadronic reactions: only one experiment clearly shows the presence of such jets in an unbiased manner, independent of geometric biases due to the limited acceptance of the detectors [4]. The essential difficulty in purely hadronic interactions is the presence of the large flux of forward-backward particles at low p_T. These diffractive and other low p_T effects dominate the hadronic cross sections, and thus jet analyses aimed at studying parton interactions must consider high p_T particles which are much rarer than those at low p_T.

It is of interest to compare the jet structure observed in e^+e^- annihilations into hadrons with possible jet structure in purely hadronic interactions. Since the quark and gluon fragmentation functions are expected to be identical in the two cases, any differences would probe details of the jet production mechanism. Such a comparison has been performed using pp collision data taken with a minimum bias trigger (as defined below) in the CERN Intersecting Storage Rings (ISR) in which one final-state leading proton has been selected [5]. In that work an attempt has been made to account for the observed difference between pp and e^+e^- interactions through the difference in baryon number. Specifically, a leading proton was selected, and the analysis was performed on only those other hadrons in the same centre-of-mass hemisphere as the leading proton. In the present work on pp interactions we insist on a selection of <u>both</u> leading protons, and perform the jet analysis on the entire B = 0 mesonic system remaining after the removal of the two leading protons.

The experiment was performed at the CERN ISR at $\sqrt{s}$ = 62 GeV, using the Split Field Magnet (SFM) detector, a device which allows one to measure the momenta of charged particles in nearly the full solid angle of 4π steradians. The detector is built around a magnet with a maximum field strength of 1 Tesla surrounding interaction region I4 of the ISR. The magnetic volume is filled with Multiwire Proportional Chambers (MWPC)

divided into three telescopes: two forward telescopes, [6] each consisting of 14 MWPC and a vertex detector, described in ref. [7]. Information about the performance of the detector can be found in previous publications [8].

The MWPC's were used in a self-triggering mode [9]. Wires of the MWPC were associated in groups of 256 to deliver fast signals which were combined to define the event trigger. This experiment used a "minimum bias" trigger, which was defined by a fast majority coincidence of at least three chambers in any of the three telescopes. This trigger essentially required the presence of at least one reconstructible track. After the exclusion of elastic events, the cross section detectible by this trigger amounts to $\sim$ 95% of the inelastic cross section. In this analysis a sample of 390 000 such minimum-bias events were used.

The raw data were processed through the SFM off-line computer program chain [10] for track finding, track reconstruction, and vertex fitting. Events with probable protons were then selected, using the criteria that the particle in either hemisphere with the largest longitudinal momentum with respect to the beam direction should be positively charged, and should have a value of $x = 2p_L^*/\sqrt{s}$ between 0.44 and 0.82 in magnitude. The quantity p_L^* is the component of the particle's momentum along the beam direction in the overall centre-of-mass frame. Since no direct particle identification was available over most of the kinematic region, the lower limit on x was suggested by the inclusive particle distributions. At $x \simeq 0.4$ the π^+ production rate is comparable to that of the protons. As x increases in magnitude, the p/π^+ ratio increases sharply, and so the assumption that the leading positive particle is a proton becomes more accurate. The upper limit on x was chosen to remove all diffractive events. In addition, a momentum error cut $\Delta p/p < 0.08$ was required for this leading particle. From the inclusive single particle distributions [11] we estimate that the sample of "leading protons" thus chosen is 85% pure. For this analysis we select only those events in which we detect one leading proton in each of the hemispheres with respect to the beam axis. These form a sample of 3283 events. These data were corrected for geometrical acceptance losses in the detector, losses due to decay and secondary interactions, and inefficiencies of the analysis chain. The average total correction factor applied to the data is about 1.4.

In order to compare properly the pp interaction data with data on e^+e^- annihilations, it is necessary not only to remove the two identified protons so that we are comparing B = 0 systems, but also to transform all momenta into the rest frame of the mesonic system. This can be done using knowledge of the incident beam momenta and the momenta of the two leading protons. Lack of knowledge of missing neutral particles plays no role as yet. In the rest frame of the mesonic system the event appears as sketched in fig. 1. The two beam particles, p_1 and p_2 transfer equal and opposite momenta to the meson system. The dashed lines represent momentum transferred, and not specific particles.

The quantity which corresponds to $\sqrt{s}$ in e^+e^- annihilations is the invariant mass of the mesonic system, M_0, and this too can be calculated entirely from the known beam and proton momenta without reference to possible missing neutrals. Due to the finite range of allowed x over which protons are selected, there is a distribution of values for the invariant mass of the mesonic system, as shown in fig. 2. Fig. 3 shows the distributions in sphericity for the events in five regions of invariant meson mass: (a) $M_0 < 18$ GeV, (b) 18 GeV $< M_0 <$ 22 GeV, (c) 22 GeV $< M_0 <$ 26 GeV, (d) 26 GeV $< M_0 <$ 30 GeV, and (e) $M_0 > 30$ GeV. Sphericity is defined as

$$S = \frac{3}{2} \text{ Min } \frac{\sum_i |p_T^i|^2}{\sum_i |p^i|^2} ,$$

where p_T^i refers to the component of the i^{th} particle's momentum transverse to the jet axis, p^i to the magnitude of the i^{th} particle's momentum, the sums over i are over all final state particles in the B = 0 mesonic system, and the minimization refers to all possible orientations of the jet axis. Fig. 4 shows the average sphericity as a function of M_0, along with the e^+e^- annihilation data from the TASSO Collaboration [12]. Although the two cases are similar, the average sphericity in this experiment is consistently somewhat below that in the e^+e^- case. Also shown in fig. 4 are the predictions of a longitudinal phase space model, which agree well with the data of this experiment. Details of the model are discussed below.

Fig. 5 shows the distributions in sphericity versus the quantity y for all events. Let $\vec{p}_j$ be the momentum of the j^{th} hadron in the B = 0 system

in the overall rest frame of this system, and let p_j^α be its rectangular components, $\alpha = x, y, z$. Then we may define the momentum tensor as $T_{\alpha\beta} = \sum_j p_j^\alpha p_j^\beta$, and obtain the three eigenvalues λ_1, λ_2, and λ_3 of this tensor. We define $Q_K = \lambda_K/(\lambda_1 + \lambda_2 + \lambda_3)$, arranged such that $0 \leq Q_1 \leq Q_2 \leq Q_3$. The sphericity, S, is $S = 3(Q_1 + Q_2)/2$, the aplanarity A, is defined as $A = 3Q_2$, and the quantity y, which is the difference between the width and flatness of the momentum distribution is defined as $y = \sqrt{3}(Q_2 - Q_1)/2$. The jet axis is defined as being along that eigenvector of $T_{\alpha\beta}$ which corresponds to the largest eigenvalue. We see that the bulk of our events are at low sphericity which is the region of 2-jet events, but there are some events at large sphericity but small aplanarity, which are planar events; and even a small number of spherical events at large sphericity and large aplanarity. In very general terms this distribution is similar to that observed in e^+e^- annihilation into hadrons at PETRA, but there are significant differences in detail, as mentioned earlier in regard to the sphericity distribution. No significant changes in this distribution are observed as a function of M_0.

In fig. 6 we show the distributions in p_T^2, where p_T^2 is the square of the individual hadron's momentum transverse to the jet axis. The five distributions refer to the same five regions of M_0 as in fig. 3. We observe no significant change in the shape of the p_T^2 distribution with M_0. This is most clearly seen in fig. 7, which shows the distributions in p_T^2 in the lowest and highest regions of M_0.

Fig. 8 shows the average value of p_T^2 as a function of M_0. The data of this experiment show no dependence on M_0. In contrast, the data of the TASSO Collaboration, [12] also shown in fig. 8 show a pronounced dependence of $\langle p_T^2 \rangle$ on $\sqrt{s}$. This is generally interpreted to be a sensitive test of quark-quark-gluon jets(*). The predictions of the longitudinal phase space model are shown as the smooth curve in fig. 8. They agree well with the data of this experiment, in particular in the absence of a strong dependence on M_0.

(*) We note that a recent prediction of the energy dependence of $\langle p_T^2 \rangle$ in pp collisions by L. Angelini et al. [13] shows much less energy dependence than observed in e^+e^- collisions by the TASSO Collaboration, and is in good agreement with our data. This is shown as the dashed curve in fig. 8.

In fig. 9 we show the distributions in $\langle p_T^2 \rangle_{in}$ and $\langle p_T^2 \rangle_{out}$, where $\langle p_T^2 \rangle_{in/out}$ are the averages of the squares of the momenta transverse to the jet axis and in/out of the event plane. The event plane is defined as the plane formed by the two eigenvectors corresponding to the two largest eigenvalues of the momentum tensor, $T_{\alpha\beta}$, defined above. In each case the distribution in $\langle p_T^2 \rangle_{in}$ is significantly broader than that in $\langle p_T^2 \rangle_{out}$, but this is expected from the definitions:

$$\langle p_T^2 \rangle_{out} = \frac{\Lambda_1}{N}$$

and

$$\langle p_T^2 \rangle_{in} = \frac{\Lambda_2}{N}$$

where Λ_1 is the smallest eigenvalue and Λ_2 is the middle eigenvalue of the momentum tensor, $T_{\alpha\beta}$, and N is the number of particles whose momenta are included in the tensor. The data are well-reproduced by the predictions of the longitudinal phase space model. We furthermore observe that there is no significant broadening of either the $\langle p_T^2 \rangle_{in}$ or $\langle p_T^2 \rangle_{out}$ distributions with increasing M_0. This is most clearly seen in fig. 10, which shows the distributions in $\langle p_T^2 \rangle_{in}$ for the lowest and highest regions of M_0. This result is in disagreement with that of ref. [5] which claims such an energy dependence for $\langle p_T^2 \rangle_{in}$.

In fig. 11 we show the angular distributions of the sphericity or jet axis with respect to the direction of the momentum transfers to the B = 0 mesonic system as shown in fig. 1. The data in fig. 11 do not show the characteristic $1 + \cos^2\theta$ angular distribution expected from a one-photon intermediate state and seen in e^+e^- annihilations, but instead are sharply peaked in the forward direction. This is just the behaviour expected if the secondary particles are produced largely in the forward-backward direction, as for example in a model of phase space with limited transverse momenta. This distribution does not change significantly with M_0. The dashed line corresponds to the predictions of the longitudinal phase space model.

In figs 12 and 13 we show the quantities E_{vis}/E_{tot} and $\langle n_c \rangle$ as functions of M_0. E_{vis} is the visible (i.e., charged) energy in the overall

centre of mass assuming all particles are pions in the B = 0 system, while E_{tot} is the total energy in this system obtained from subtracting the energies of the two identified protons from the total c.m. energy. Clearly, therefore E_{vis}/E_{tot}, thus calculated, is an underestimate of its true value. In any case, E_{vis}/E_{tot} appears to decrease with increasing M_0, while $\langle n_c \rangle$, the average charge multiplicity in the B = 0 system, increases sharply with M_0. In both cases the predictions of the longitudinal phase space model (smooth curves) agree well with the data.

The absence of any significant M_0 dependence of $\langle p_T^2 \rangle$ of the individual hadrons with respect to the sphericity axis (fig. 8), and the sharp angular dependence of the sphericity axis itself (fig. 11) suggest that a model of cylindrical or longitudinal phase space with limited transverse momenta might explain these data. The model chosen had the following inputs:

(a) Charge multiplicity distribution from the measured distribution of minimum-bias events at $\sqrt{s}$ = 62 GeV at the ISR;

(b) Neutral multiplicity distribution from 300 GeV/c pp Fermilab bubble chamber data [14], scaled in energy;

(c) Longitudinal momenta flat in x; and

(d) Transverse momenta distributed according to $e^{-4.5M_T}$ for each particle, with $M_T = \sqrt{p_T^2} + M2$, in which p_T is the component of the particle's momentum transverse to the incident direction, i.e. M_T is the transverse mass of the hadron. This distribution reproduces the observed inclusive distribution in transverse momentum.

The model also imposed conservation of the electric charge and conservation of energy and momentum in the generation of all Monte-Carlo events, although neutral particles were then discarded in the physics analysis in order to simulate the actual experiment conditions.

In conclusion, we have examined minimum bias proton-proton interactions at the highest available energies at the ISR and have subtracted

off the identified protons. The resultant B = 0 system has been analyzed in terms of standard jet-type analyses and compared with data on e^+e^- annihilations into hadrons. In contrast to previous results [5] we find significant difference between the purely hadronic and e^+e^- data, especially in the energy dependence of $\langle p_T^2 \rangle$ of the individual hadrons with respect to the sphericity axis. We interpret this to mean that the impulse model and the other approximations which are used to interpret the purely hadronic data are sufficiently important to cause the observed differences between the hadronic data and the simpler case of e^+e^- annihilation into a virtual photon which then produces a $q\bar{q}$ pair. Furthermore, the predictions of the longitudinal phase space model are in good agreement with the data of this experiment.

We thank the technical staff of the SFM goup for all their efforts. We also thank U. Schlüpmann for assistance with the data, and M. J. Puhala for many helpful discussions. This work was supported in part by the U.S. Department of Energy under contract W-7405-eng-82. The Heidelberg and Dortmund groups have been supported in part by the Bundesministerium für Forschung und Technologie of the Federal Republic of Germany.

REFERENCES

[1] R.I. Schwitters et al., Phys. Rev. Lett. 35 (1975) 1320;
G. Hansen et al., Phys. Rev. Lett. 35 (1975) 1609.

[2] PLUTO Collaboration, Ch. Berger et al., Phys. Lett. 78B (1978) 176.

[3] TASSO Collaboration, R. Brandelik et al., Phys. Lett. 86B (1979) 243;
MARK J Collaboration, D.P. Barber et al., Phys. Rev. Lett. 43 (1979) 830;
PLUTO Collaboration, Ch. Berger et al., Phys. Lett. 86B (1979) 418;
JADE Collaboration, W. Bartel et al., Phys. Lett. 91B (1980) 142.

[4] CCHK Collaboration, D. Drijard et al., Nucl. Phys. B155 (1979) 269;
CCHK Collaboration, D. Drijard et al., Nucl. Phys. B156 (1979) 309.

[5] M. Basile et al., Phys. Lett. 92B (1980) 367;
M. Basile et al., Planar jets in pp collisions, CERN/EP 80-113, 27 June 1980 (Madison);
M. Basile et al., The energy dependence of charged particle multiplicity in pp collisions, CERN/EP 80-112, 27 June 1980 (Madison);
M. Basile et al., The fractional momentum distribution in pp collisions compared to e^+e^- annihilation, CERN/EP 80-111, 27 June 1980 (Madison).

[6] R. Bouclier et al., Nucl. Instr. and Meth. 115 (1974) 235.

[7] R. Bouclier et al., Nucl. Instr. and Meth. 125 (1975) 19.

[8] CCHK Collaboration, M. Della Negra et al., Nucl. Phys. B127 (1977) 1;
W. Bell et al., Nucl. Instr. and Meth. 156 (1978) 111.

[9] W. Bell et al., Nucl. Instr. and Meth. 125 (1975) 437.

[10] M. Della Negra and A. Norton (unpublished), adpted from H. Wind, Function parametrization, Proc. CERN computing and data processing school, Yellow Report CERN 72-21;
D. Drijard, SPLINE track fit, SFM internal Note 1976, adapted from H. Wind, CERN/NP/DHG 73-5 (1973).

[11] J.W. Chapman et al., Phys. Rev. Lett. 32 (1974) 257;
P. Capiluppi et al., Nucl. Phys. B70 (1974) 1;
J. Singh et al., Nucl. Phys. B140 (1978) 189.

[12] TASSO Collaboration, R. Brandelik et al., Phys. Lett. 89B (1980) 418;
TASSO Collaboration, R. Brandelik et al., Phys. Lett. 83B (1979) 261.

REFERENCES (Cont'd)

[13] L. Angelini et al., The structure of final states in low p_T pp-interactions at high energies, BARI-GT/81-05, April 1981.

[14] A. Sheng et al., Phys. Rev. D11 (1975) 1733

FIGURE CAPTIONS

Fig. 1 Diagram of the "two-proton" events.

Fig. 2 Invariant mass of the B = 0 mesonic system after the removal of the two identified protons.

Fig. 3 Distributions in sphericity for the events: (a) $M_0 < 18$ GeV, (b) 18 GeV $< M_0 <$ 22 GeV, (c) 22 GeV $< M_0 <$ 26 GeV, (d) 26 GeV $< M_0 <$ 30 GeV, and (e) $M_0 > 30$ GeV.

Fig. 4 Average sphericity as a function of M_0. Also shown are data from the TASSO Collaboration [12]. The smooth curve shows the prediction of a longitudinal phase-space model.

Fig. 5 Distribution of events as a function of sphericity and aplanarity, for all values of M_0.

Fig. 6 Distribution in p_T^2 of the individual hadrons with respect to the jet axis. The five regions of M_0, a through e, are the same as in fig. 3.

Fig. 7 Distributions in p_T^2 of the individual hadrons with respect to the jet axis for the lowest and highest regions of M_0.

Fig. 8 Average value of p_T^2 as a function of M_0. Also shown are data from the TASSO Collaboration [12]. The solid curve shows the prediction of a longitudinal phase-space model, and the dashed curve that of the model of L. Angelini et al., [13].

Fig. 9 Distribution in $\langle p_T^2 \rangle_{in/out}$ with respect to the jet axis in/out of the "event plane": (a) All M_0, and (b) $M_0 > 30$ GeV. In (b) are also shown data from the TASSO Collaboration [12]. The smooth curves show the predictions of the longitudinal phase-space models.

Fig. 10 Distribution in $\langle p_T^2 \rangle_{in}$ with respect to the jet axis in the "event plane" for the lowest and highest regions of M_0.

FIGURE CAPTIONS (Cont'd)

Fig. 11 Angular distribution of the jet axis with respect to the momentum-transfer line of flight of the two protons. The dashed line shows the prediction of the longitudinal phase-space model.

Fig. 12 E_{vis}/E_{tot} as a function of M_0. The smooth curve shows the prediction of the longitudinal phase-space model.

Fig. 13 $\langle n_c \rangle$ as a function of M_0. Also shown are data from the TASSO Collaboration [12]. The smooth curve shows the prediction of the longitudinal phase-space model.

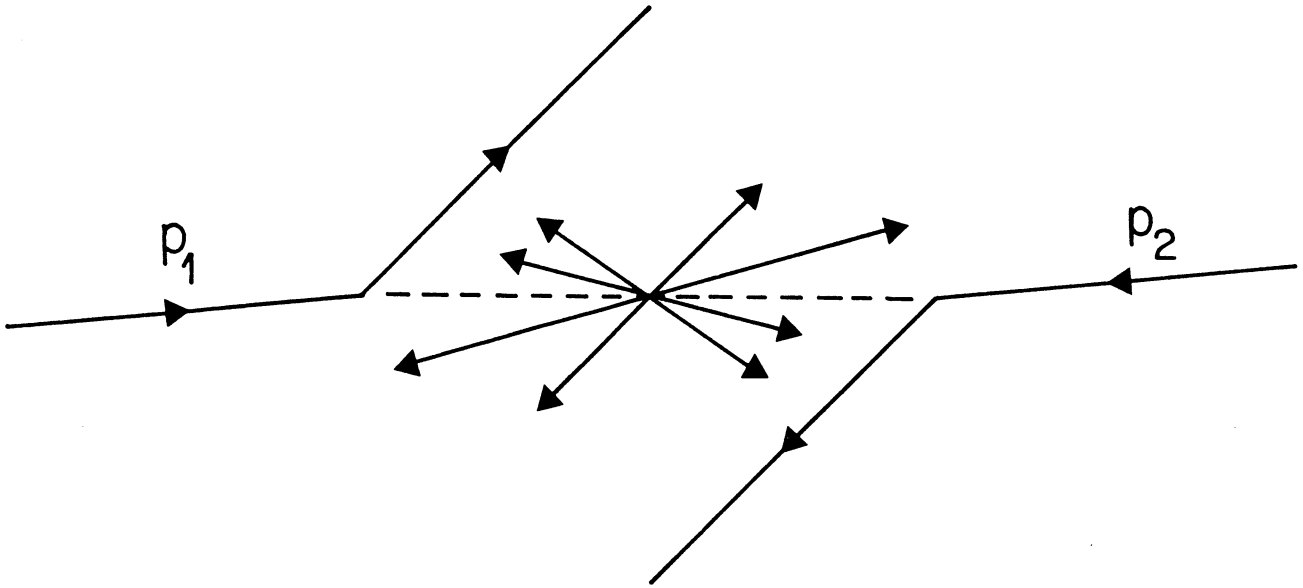

Fig. 1

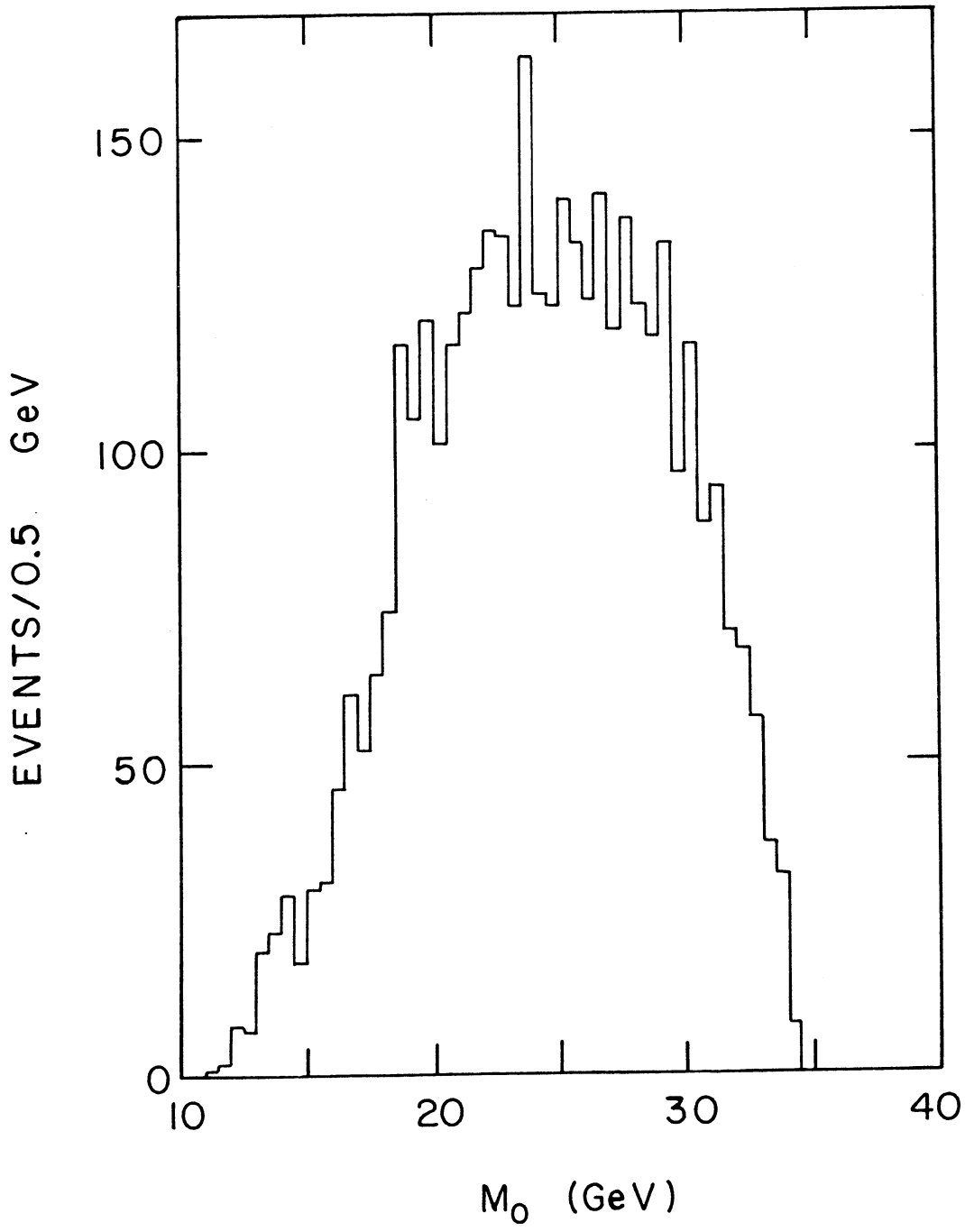

Fig. 2

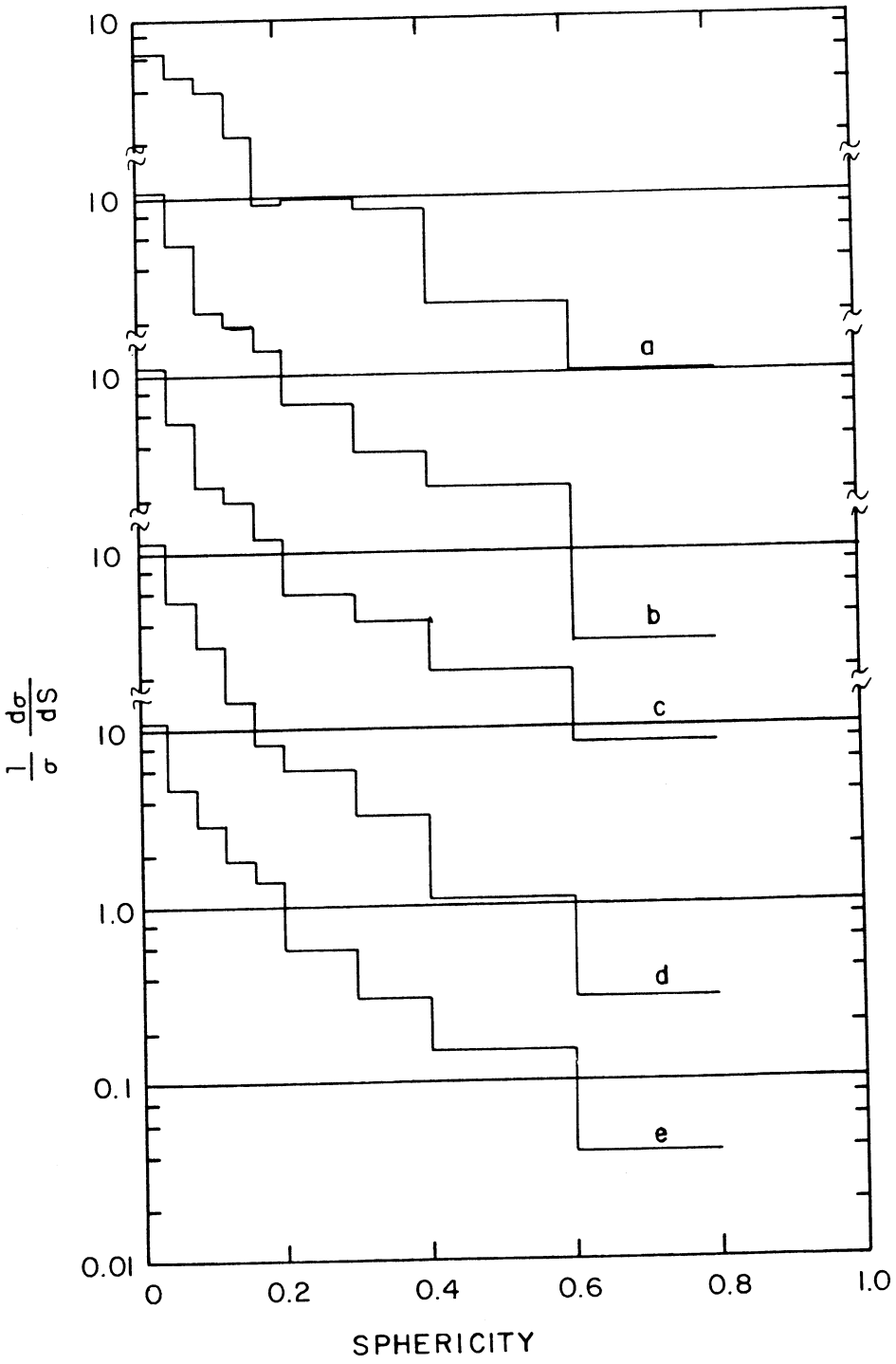
10
10
10
10
10
1.0
0.1
0.01
a
b
c
d
e
0
0.2
0.4
0.6
0.8
1.0
SPHERICITY
$\frac{1}{\sigma}\frac{d\sigma}{dS}$

Fig. 3

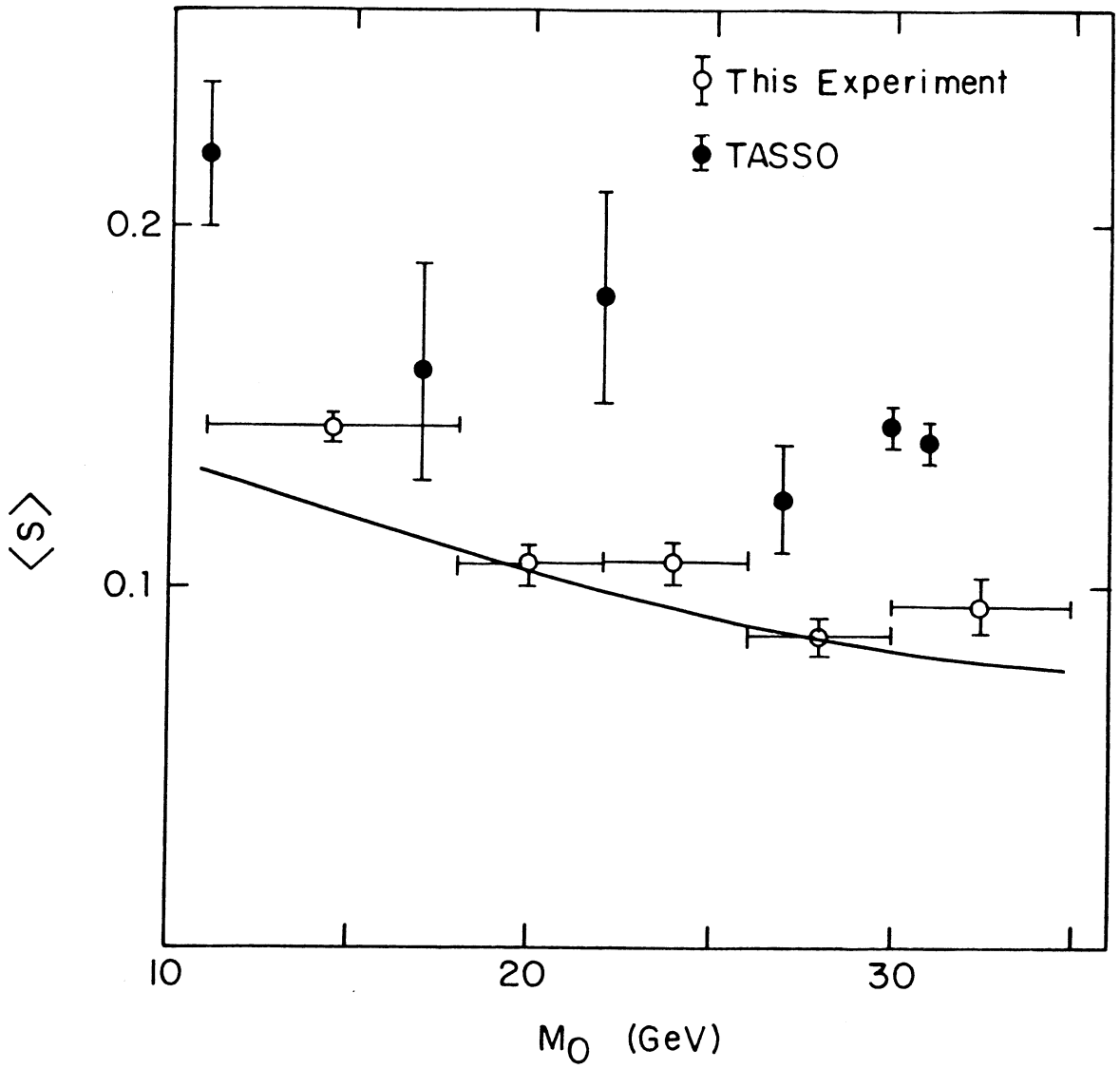

Fig. 4

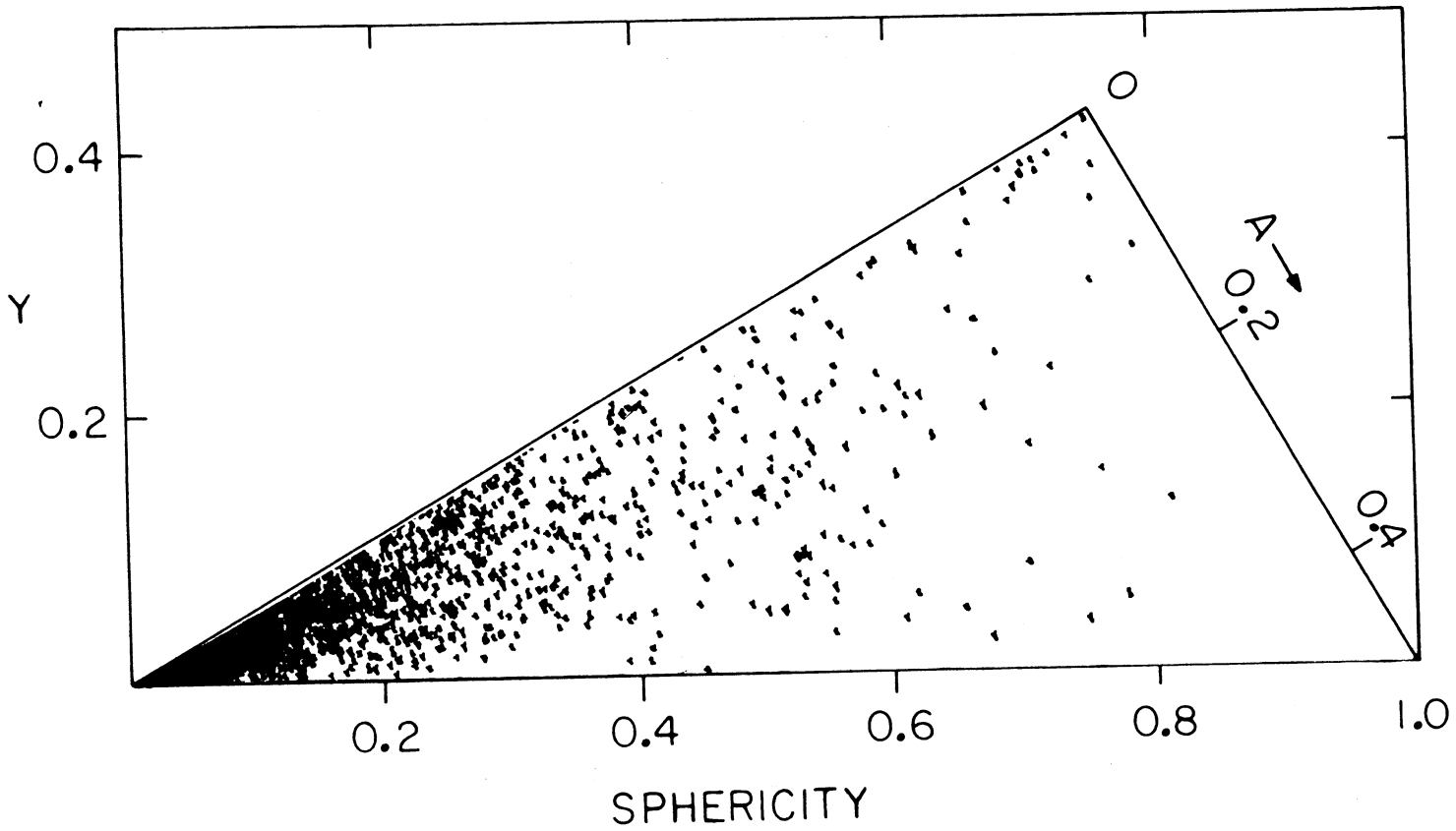

Fig. 5

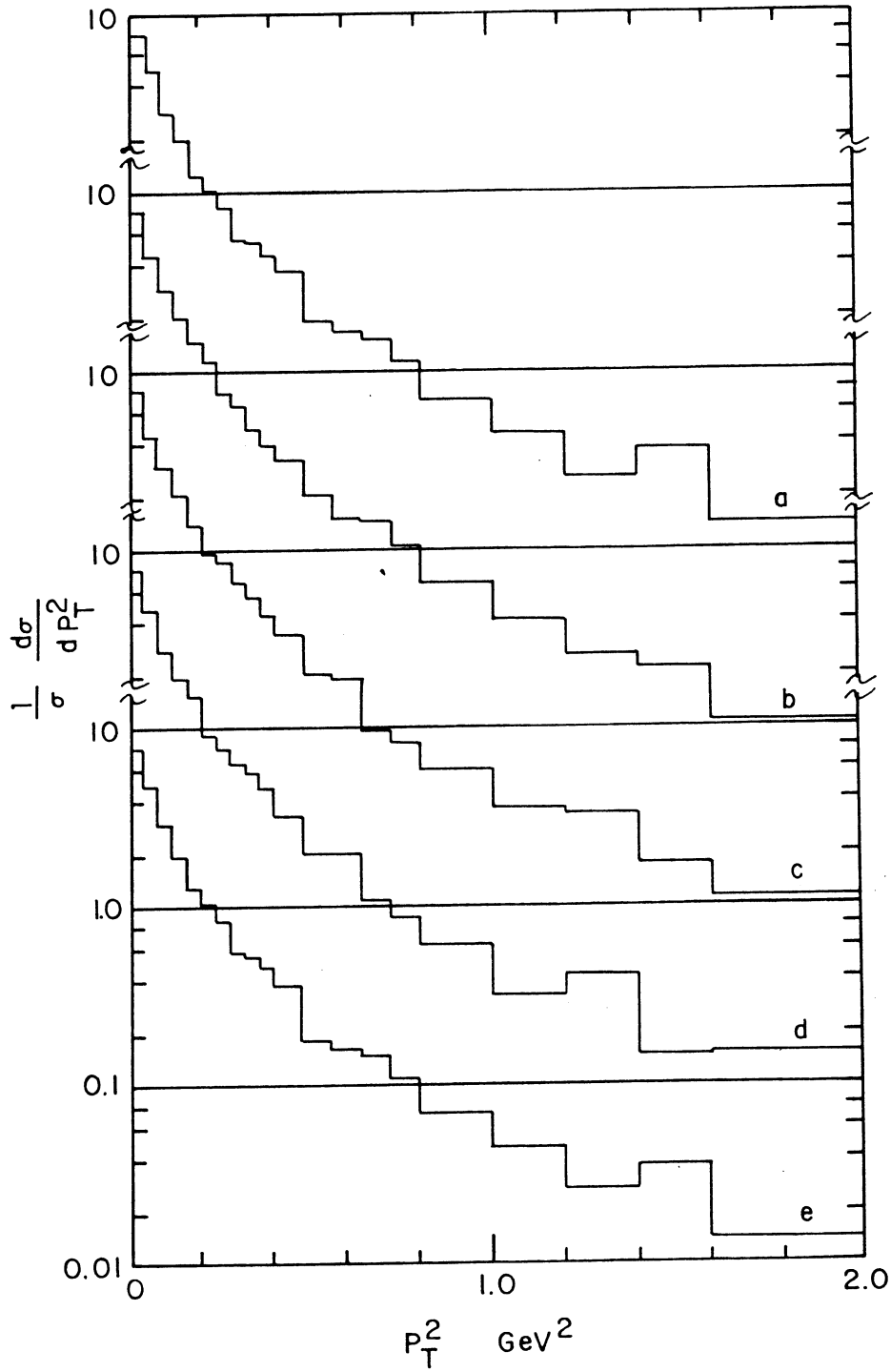
10
10
10
10
10
1.0
0.1
0.01
a
b
c
d
e
0
1.0
2.0
$\frac{1}{\sigma}\frac{d\sigma}{dP_T^2}$
P_T^2 GeV^2

Fig. 6

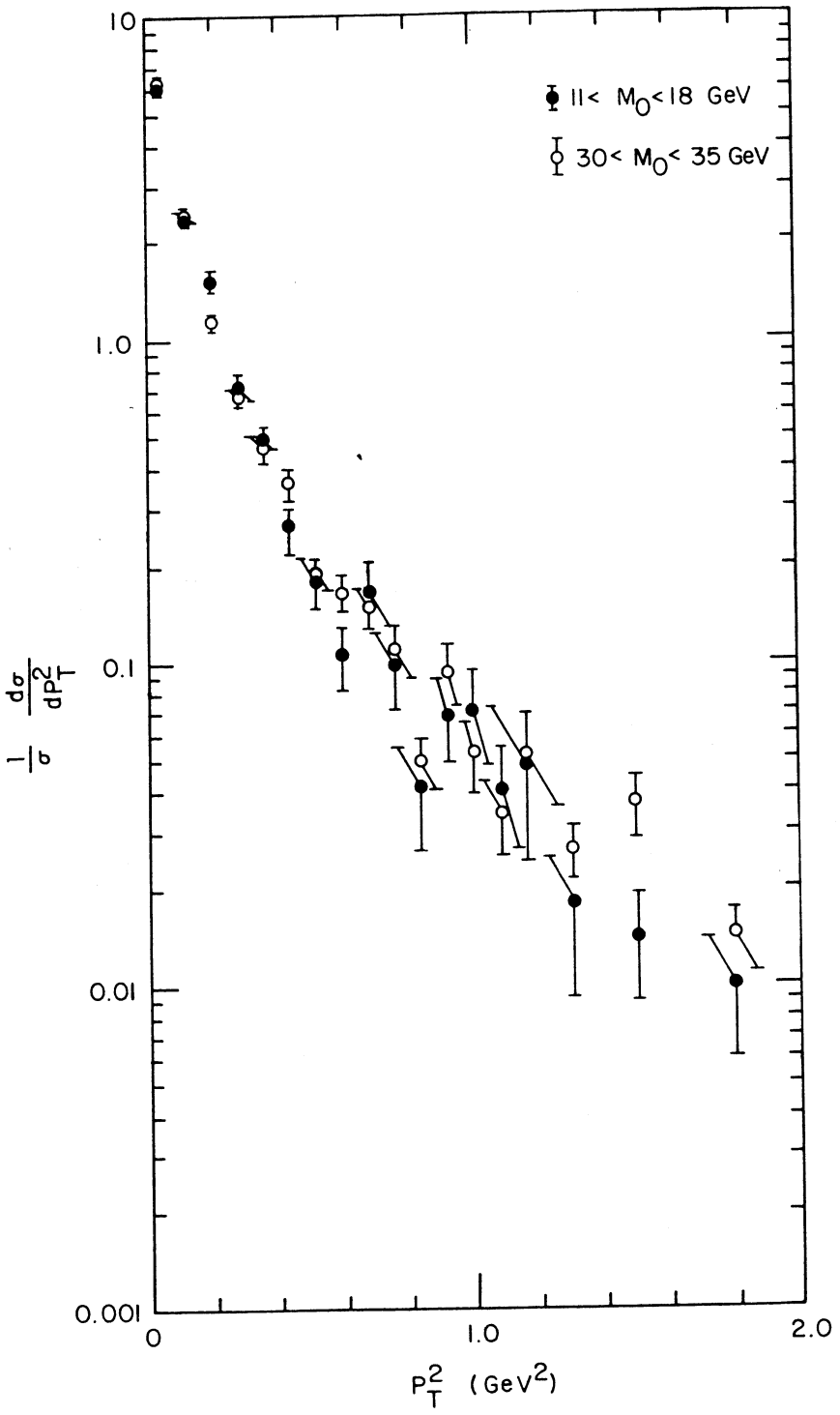
11< M_0<18 GeV
30< M_0< 35 GeV
10
1.0
0.1
0.01
0.001
0
1.0
2.0
$\frac{1}{\sigma}\frac{d\sigma}{dP_T^2}$
P_T^2 (GeV^2)

Fig. 7

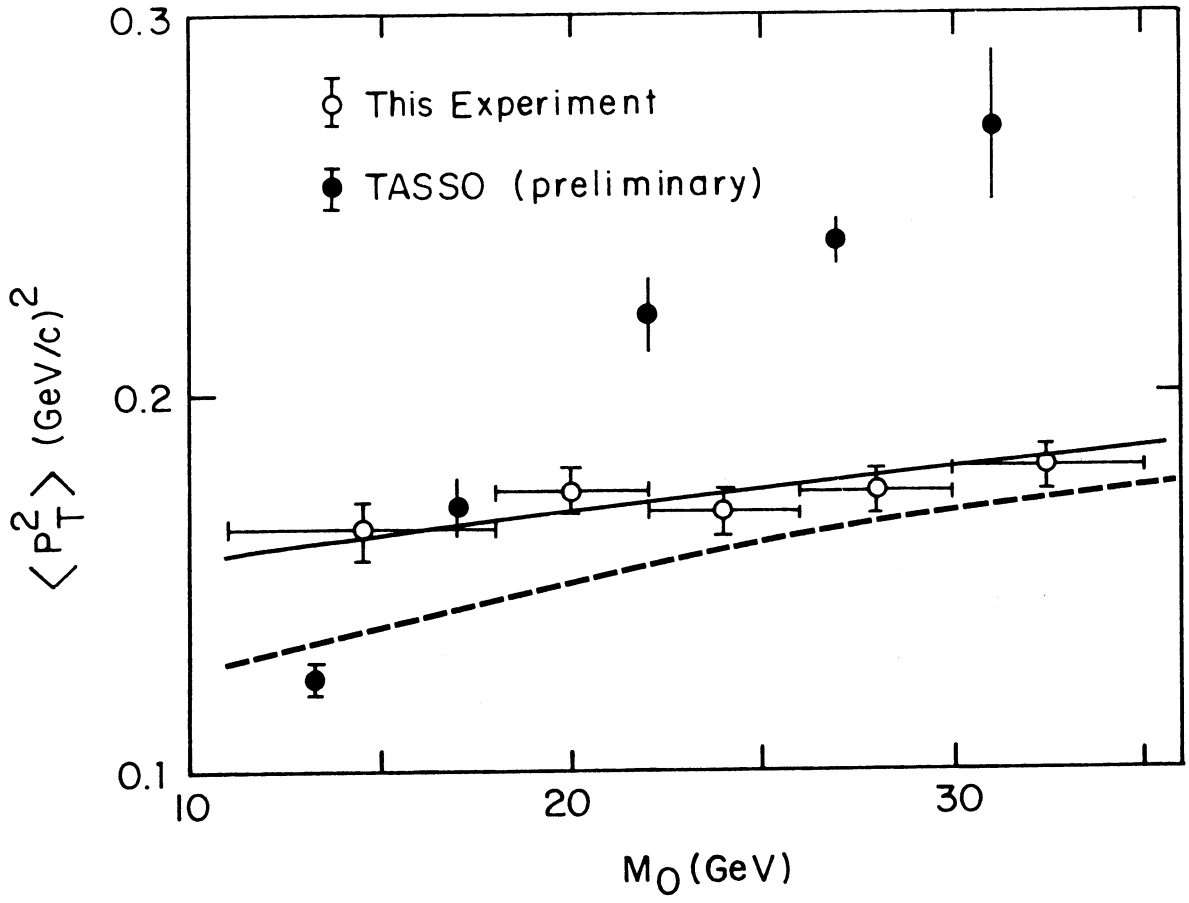
0.3
0.2
0.1
10
20
30
This Experiment
TASSO (preliminary)
$\langle P_T^2 \rangle$ (GeV/c)^2
M_O (GeV)

Fig. 8

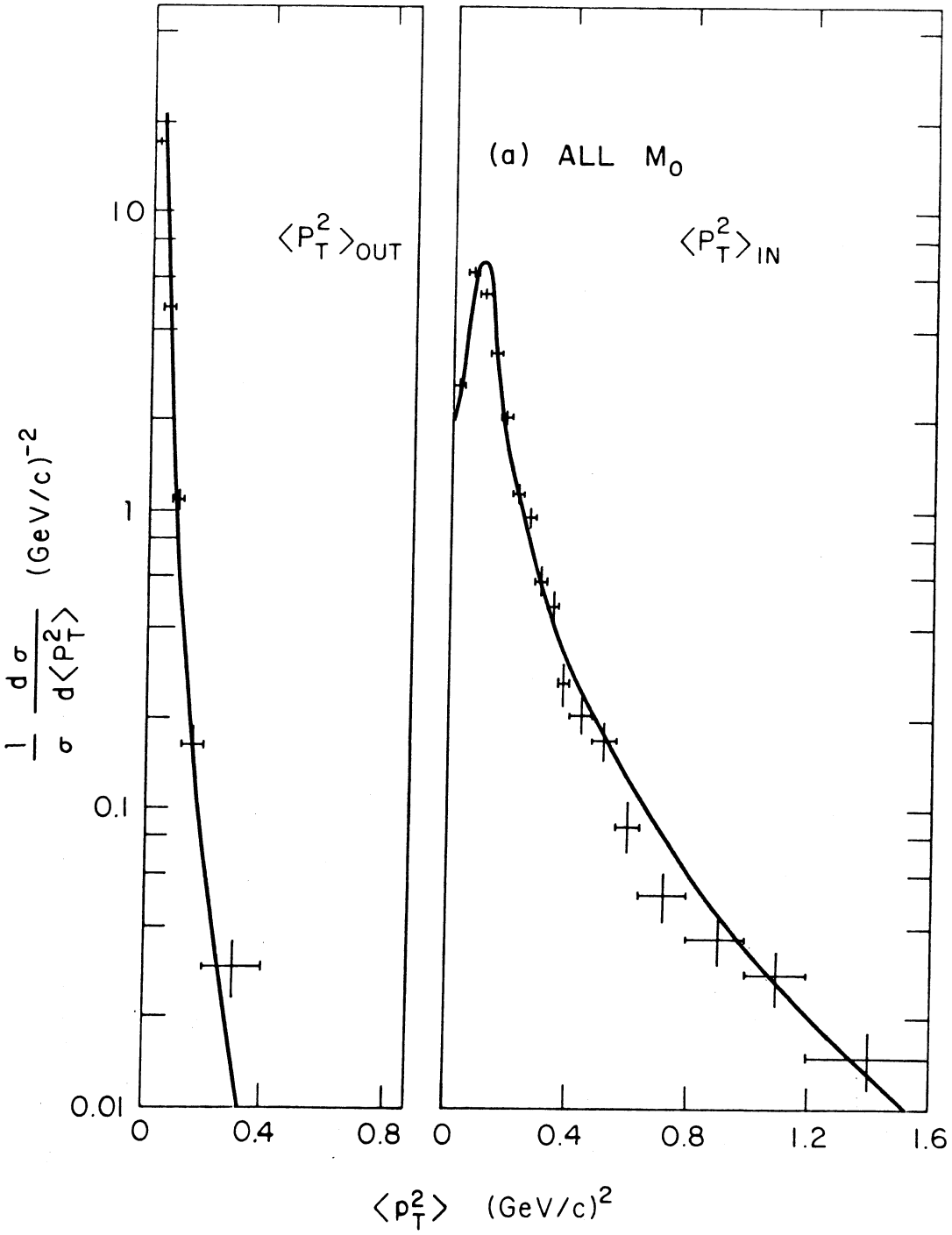
(a) ALL M_0
$\langle P_T^2 \rangle_{OUT}$
$\langle P_T^2 \rangle_{IN}$
$\frac{1}{\sigma}\frac{d\sigma}{d\langle P_T^2 \rangle}$ $(GeV/c)^{-2}$
10
1
0.1
0.01
0
0.4
0.8
0
0.4
0.8
1.2
1.6
$\langle p_T^2 \rangle$ $(GeV/c)^2$

Fig. 9(a)

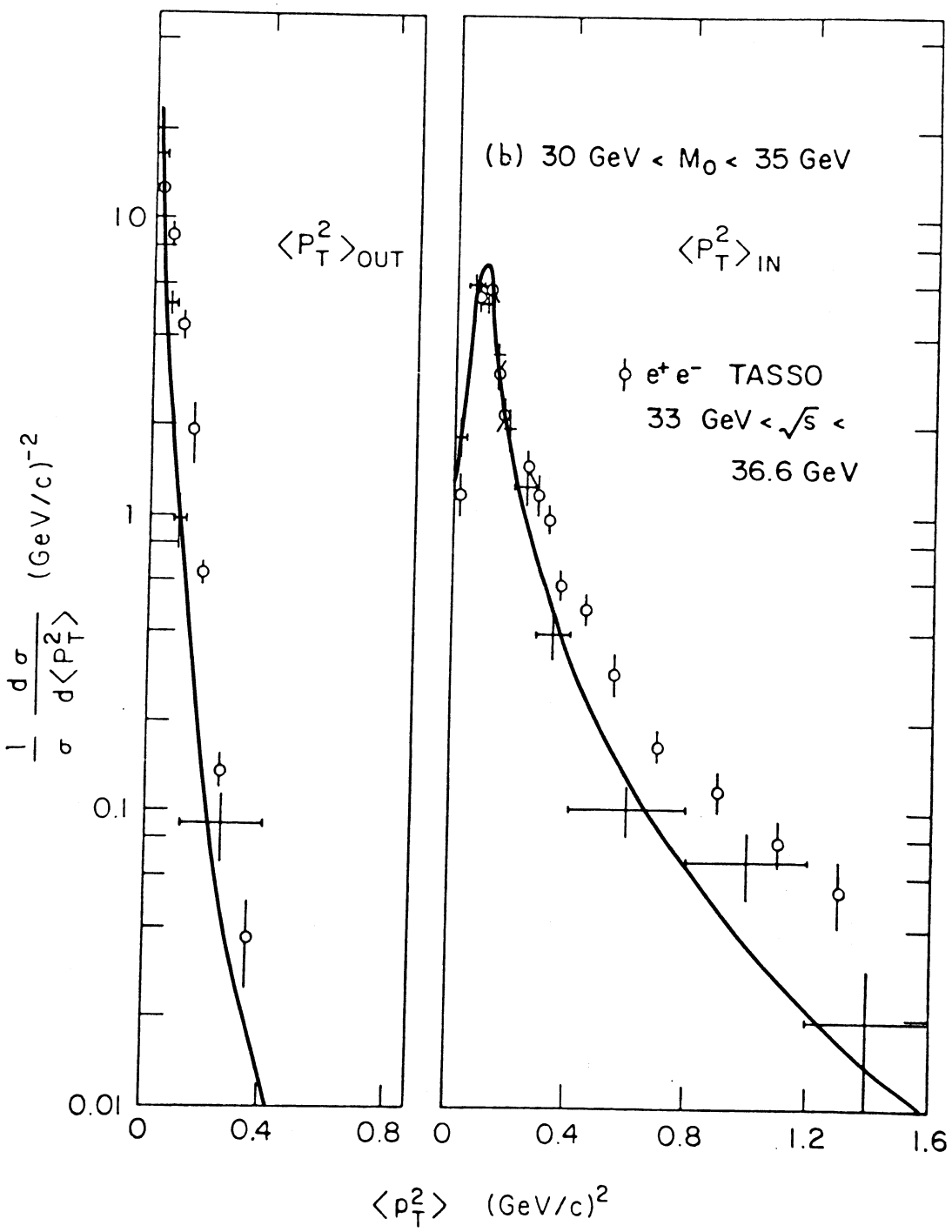
(b) 30 GeV < M_0 < 35 GeV
$\langle P_T^2 \rangle_{OUT}$
$\langle P_T^2 \rangle_{IN}$
e^+e^- TASSO
33 GeV < $\sqrt{s}$ < 36.6 GeV
$\frac{1}{\sigma}\frac{d\sigma}{d\langle P_T^2\rangle}$ $(GeV/c)^{-2}$
10
1
0.1
0.01
0
0.4
0.8
1.2
1.6
$\langle p_T^2 \rangle$ $(GeV/c)^2$

Fig. 9(b)

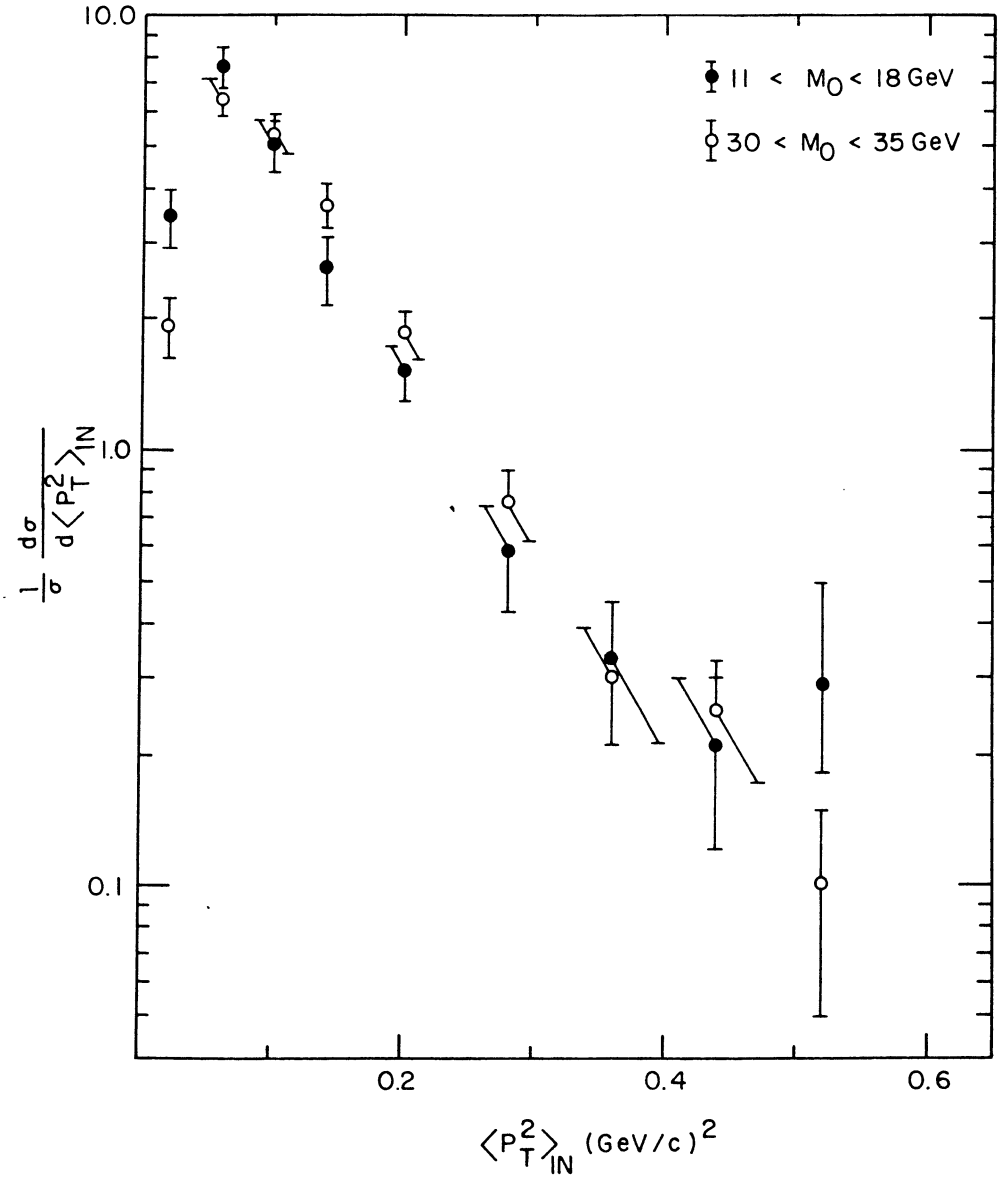
10.0
1.0
0.1
0.2
0.4
0.6
11 < M0 < 18 GeV
30 < M0 < 35 GeV
$\frac{1}{\sigma}\frac{d\sigma}{d\langle P_T^2\rangle_{IN}}$
$\langle P_T^2\rangle_{IN}$ (GeV/c)^2

Fig. 10

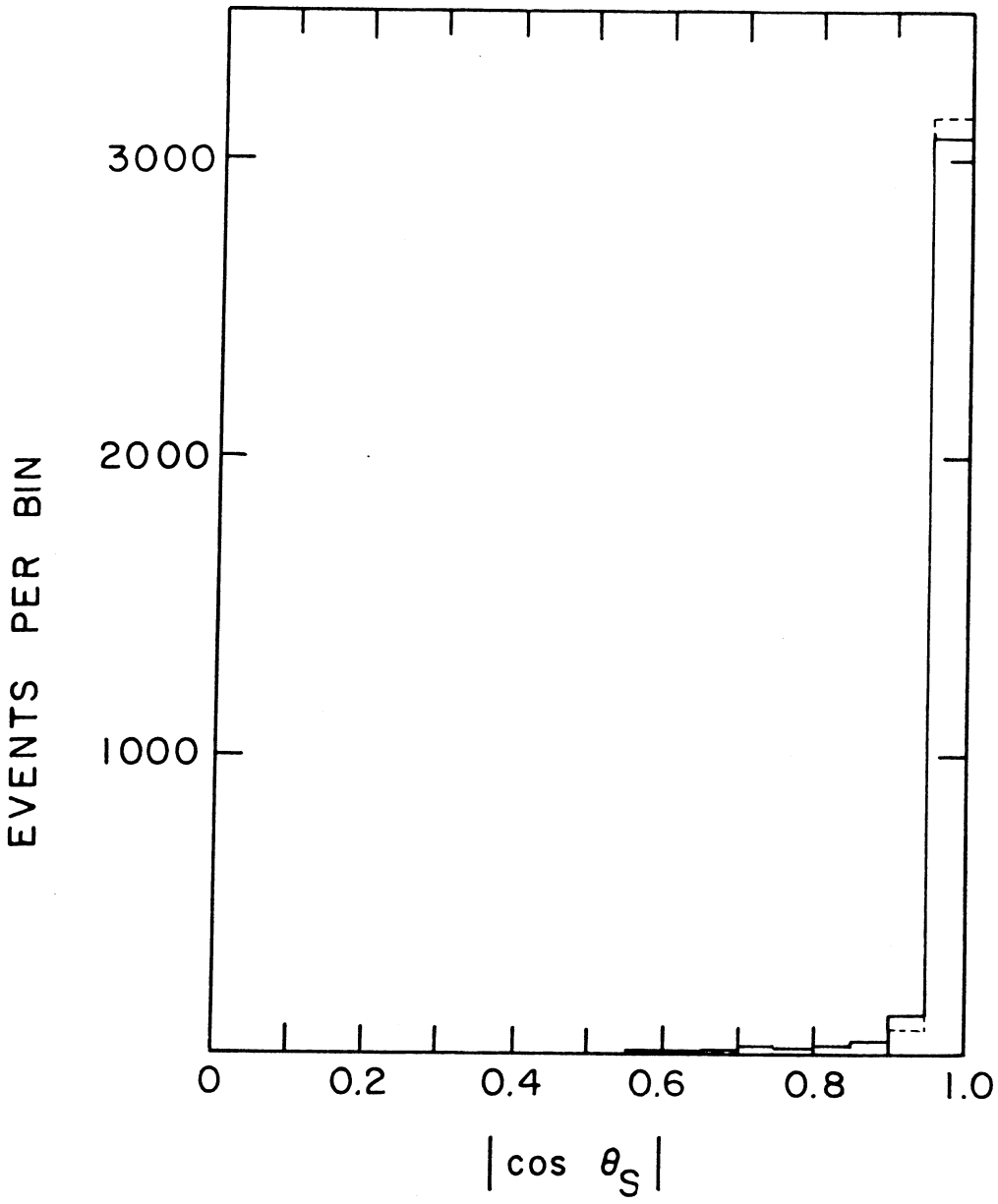

Fig. 11

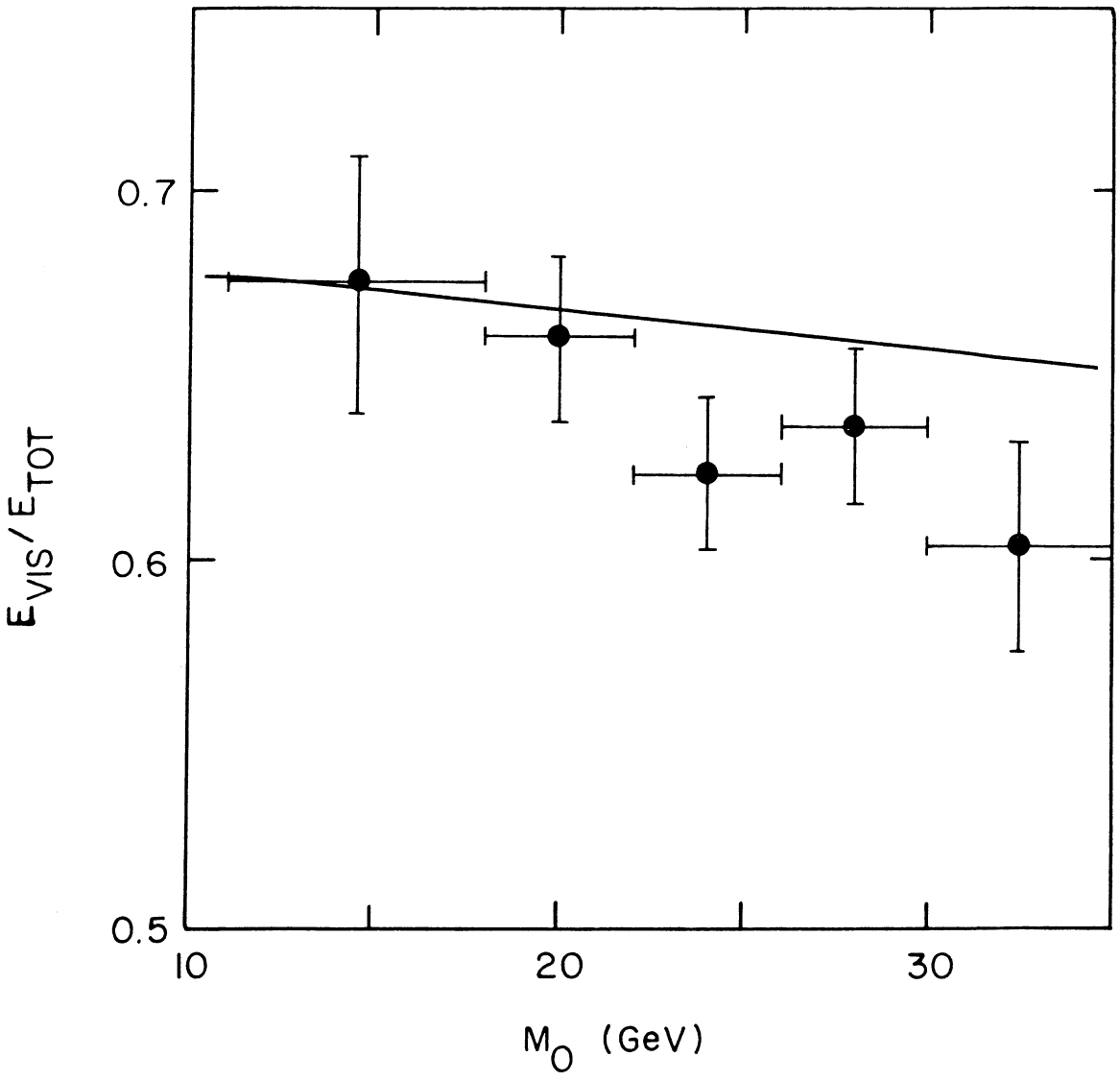

Fig. 12

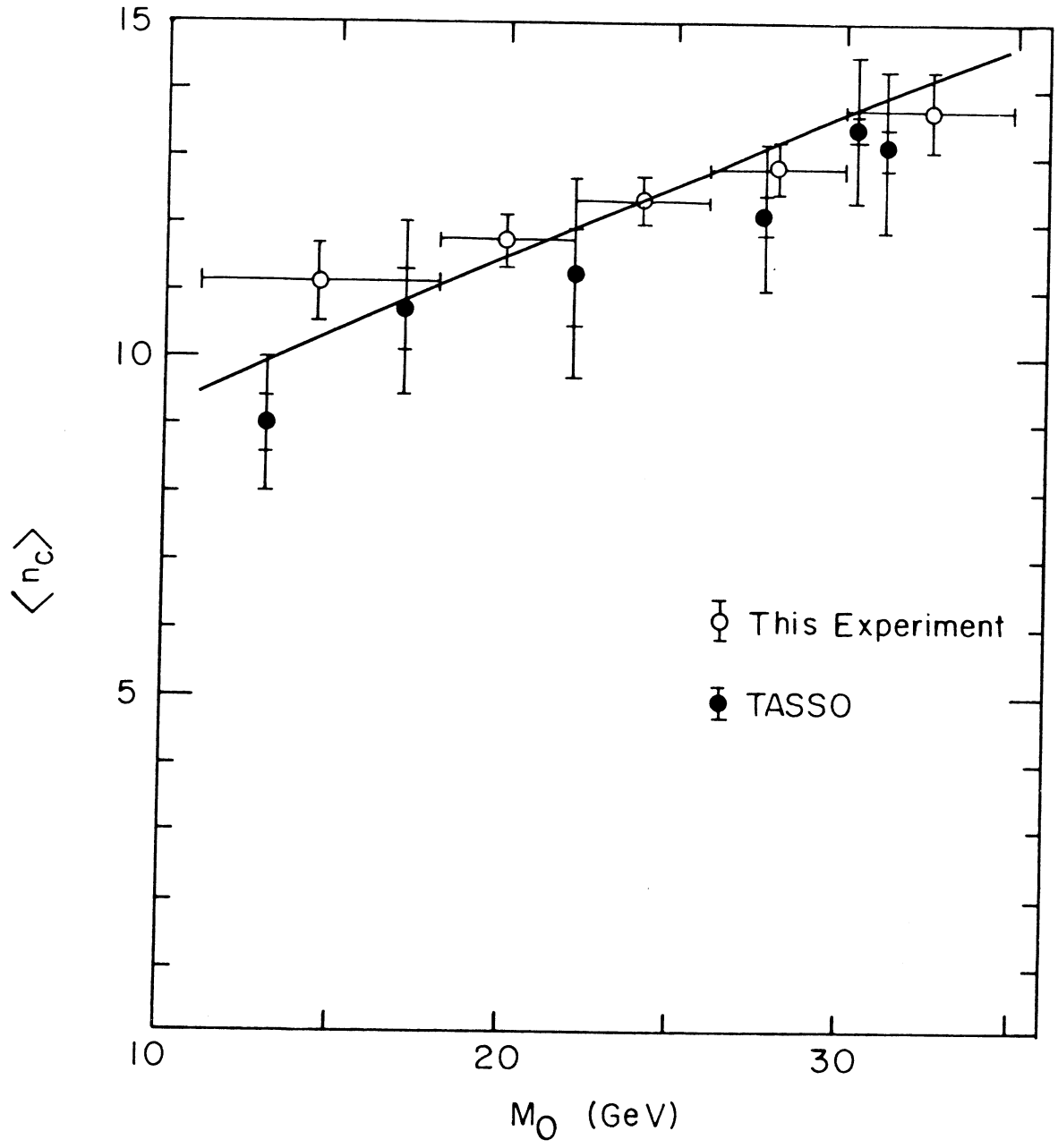

Fig. 13